Charged Higgs boson discovery prospects

Baradhwaj Coleppa,[1,*] Agnivo Sarkar,[1,†] and Santosh Kumar Rai[2,‡]

[1]*Physics Discipline, Indian Institute of Technology-Gandhinagar, Palaj Campus, Gujarat 382355, India*
[2]*Regional Centre for Accelerator-based Particle Physics, Harish-Chandra Research Institute, HBNI, Chhatnag Road, Jhusi, Prayagraj (Allahabad) 211019, India*

(Received 11 October 2019; accepted 6 March 2020; published 25 March 2020)

We study the discovery prospects of the charged Higgs boson in the context of multi-Higgs models in certain beyond the Standard Model scenarios. We classify models into three categories based on the charged Higgs coupling properties: gaugophobic, fermiophobic, and chromophobic. In each case, we identify viable modes of discovery and present LHC analysis for discovery. We find that extensions of the Standard Model in which the charged Higgs boson does not couple to colored particles offer the best possible avenues for discovery.

DOI: 10.1103/PhysRevD.101.055030

I. INTRODUCTION

The Standard Model (SM) [1] of particle physics has been a phenomenal success in describing three of the four fundamental forces, and myriad experiments have now firmly established its particle content and, to a large extent, the couplings involved. The SM engineers breaking of the electroweak gauge group $SU(2)_L \times U(1)_Y \to U(1)_{\rm em}$ via a Higgs field that develops a vacuum expectation value [2]. The last missing link in the picture—the physical Higgs boson—that the SM predicts has now been discovered at the CMS [3,4] and ATLAS [5] experiments. In spite of the various successes of the SM [6,7], the nagging issue remains that there is no fundamental explanation for the scale of electroweak symmetry breaking (EWSB) within the SM. The Higgs field, while *accommodating* EWSB, does not throw any light on the nature of EWSB itself. This is in stark contrast to the other scale in the SM, $\Lambda_{\rm QCD}$, whose value can be inferred directly via the running of the strong coupling constant till the point where g_s becomes large enough to bind quarks into color-singlet states. In addition, the SM does not have a candidate for dark matter nor can it explain neutrino masses. All such theoretical and phenomenological issues [8] have prompted theorists to try and construct models that extend the scope of the SM to address one or more of these questions—these fall under the collective banner of "beyond the Standard Model" (BSM) theories.

BSM scenarios typically involving either enlarging the SM gauge group $SU(3)_C \times SU(2)_L \times U(1)_Y$, thereby invoking additional avenues of symmetry breaking, or enlarging the particle content with nontrivial charges under the SM gauge group, or both. A particularly attractive avenue along the latter lines is one that involves enlarging the scalar sector of the SM—this can be done in a variety of ways introducing additional Higgs fields that transform under the electroweak gauge group. The simplest of such models involves introducing an additional Higgs doublet, with both Higgs fields now participating in EWSB. This class of models, called the two Higgs doublet models (2HDM) [9–12], can further be categorized depending on how the fermions couple to the two Higgs fields [13–15]. This scalar spectrum of the so-called type II 2HDM is identical to the minimal supersymmetric Standard Model (MSSM) [16]. In addition, one could also look for enlarged spectra with the Higgs field in representations other than the doublet under $SU(2)_L$. While such theories are typically constrained by a variety of theoretical and experimental factors [17], there are many nonminimal representations that are phenomenologically interesting. Typically, since the higher representations include multiple scalar particles with nontrivial T_3 and Y quantum numbers, one can typically expect, in addition to neutral scalars, singly or doubly charged Higgs bosons in such models. Examples include the Georgi-Machacek model [18–22] which includes the SM Higgs doublet and, in addition, a real Higgs triplet with $Y = 0$, supersymmetric models with extended Higgs sector models [23–27], Higgs triplet models [28,29] that preserve $\rho = 1$ at tree level [17], and many more.

In this paper, we undertake the collider study of the charged Higgs boson $H^{\pm}$ [30–32] in a model-independent

*baradhwaj@iitgn.ac.in
†agnivo.sarkar@iitgn.ac.in
‡skrai@hri.res.in

TABLE I. Possible production and decay modes of a charged Higgs boson in the three cases (the charge conjugated subprocesses are also implied). In this paper, we will pick an optimal channel for each and detail the collider phenomenology for a few chosen benchmark points.

Charged Higgs discovery modes		
Type	Production and decay	Final state
Gaugophobic	$pp \to H^+\bar{t}; H^+ \to t\bar{b}$	$jjb\bar{b}\,\bar{b}\,\ell\nu$
Chromophobic or fermiophobic	$pp \to H \to W^-H^+; H^+ \to W^+A$	$jjb\bar{b}\ell\nu$
	$pp \to H^+H^-; H^\pm \to W^\pm A$	$4b + 2l + 2\nu$
Leptophobic	$pp \to H^+\bar{t}; H^+ \to W^+A, t\bar{b}$	$jjb\bar{b}\,\bar{b}\,\ell\nu$
	$pp \to H \to W^-H^+; H^+ \to t\bar{b}$	$jjb\bar{b}\ell\nu$

fashion by categorizing BSM scenarios based on whether the charged Higgs boson is gaugophobic, chromophobic, or leptophobic—we lay out the essential details along with experimental inputs in Sec. II and identify the best case discovery modes for each. In Sec. III, we present the collider study for some chosen benchmark points and then translate the discovery potential in the context of type II 2HDM in Sec. IV. We present our conclusions in Sec. V.

II. OVERVIEW AND CURRENT LIMITS

A. Setup and strategy

Enlarged scalar sectors in various BSM scenarios can in general have different gauge charges and can also couple to fermions in the SM in different ways. While in principle many of these models also exhibit an enlarged gauge and/or matter spectrum, we restrict our attention to the simple case where the gauge group and fermionic content is purely SM-like. Even given this restriction, there are many possibilities for how the charged Higgs boson couples to the SM, and any single study that hopes to encompass the myriad model-building avenues that exist can only hope to do so by some form of broad classification of these models based on the nature of the charged Higgs couplings. In this spirit, we begin this study by analyzing three broad categories:

(i) *Gaugophobic models.*—The charged Higgs boson has no couplings to the SM electroweak gauge bosons, particularly the $W^\pm$.
(ii) *Leptophobic models.*—The charged Higgs boson does not couple to the leptons in the SM.
(iii) *Chromophobic models.*—Couplings of the charged Higgs boson to the colored particles in the SM are absent.

While our aim here is not to present an overview of models that satisfy one or more of the above criteria, we note that realizations of the different cases can be easily understood. For instance, one could design an enlarged scalar spectrum with the Higgs multiplet containing the charged Higgs boson coupling only to leptons or quarks. Similarly, there are certain classes of deconstructed models [33] in which the coupling of $H^\pm$ to $W^\pm$ and a scalar would be highly suppressed at tree level. Depending on the nature of its couplings, the charged Higgs boson will have rather different decay branching ratios (BR) and production mechanisms. Searches for the charged Higgs boson have largely been restricted to its production via $gb \to H^+t$, or via top decay: $t \to H^+b$ if $m_{H^\pm} < m_t$. In the former case, the predominant decay is to tb, while in the latter it could be $H^+ \to \tau\nu$. While other channels like $AW^\pm$ have been explored, to a large extent either the production or the decay have been one of the "standard" cases. This is clearly untenable in a general search strategy if, for example, the charged Higgs boson is chromophobic and the H^+tb vertex does not exist. Thus, at the outset, we would like to present the most viable channels in each model scenario and the rationale for the choices.

(i) *Gaugophobic.*—The absence of any vertex of the form[1] $H^\pm AW^\mp$ means that the dominant decay modes are $\tau\nu$ and $t\bar{b}$. Thus in this case we concentrate on the $gb \to H^+t$ production mode with $H^+ \to t\bar{b}$. While $\tau\nu$ can certainly be considered, the purely hadronic mode aids in cleaner reconstruction (at the cost of higher backgrounds, of course).
(ii) *Chromophobic.*—Since the $H^\pm$ does not couple to colored particles, the production channel $pp \to H^+\bar{t}$ is absent and we need to look for the $H^\pm$ as a decay product of a heavier particle like a heavy neutral scalar H. The possible s-channel mode $u\bar{d} \to H^+$ is suppressed by the small masses of the quarks and hence would not be viable. Thus, in this case, we look at $pp \to H \to W^\pm H^\mp$ with $H^\pm \to AW^\pm$.
(iii) *Leptophobic.*—In this case, the production can be either $gb \to H^+\bar{t}$ or $pp \to H \to W^\pm H^\mp$ with $H^\pm \to AW^\pm$ or $H^+ \to t\bar{b}$. Hence we will explore both the possibilities when analyzing this channel. We summarize all three cases in Table I.

We note that the above table is not an exhaustive list of possibilities for each scenario—for example, the $pp \to H^+\bar{t}; H^+ \to tb$ channel will exist for both gaugophobic and

[1]Here and in the rest of the paper, we will indicate generic heavy scalars by A and H (the typical symbols used in the 2HDM literature) and will reserve the symbol h for the SM-125 GeV Higgs boson. In our study, we do not make use of angular correlations and hence will not distinguish between scalar and pseudoscalar decay modes explicitly.

the leptophobic cases. In addition, it is seen that while the production and decay channels are quite different in the various scenarios, the final state for all of them contains multijets and b's.[2] However, the presence of $\ell + \not{E}_T$ means that all SM backgrounds have at least one electroweak vertex[3]—thus rendering the background small is less difficult compared to the scenario of a pure QCD background. On the other hand, we require high enough signal cross sections that will withstand multiple b tagging efficiencies and substantial p_T cuts—we will see in the next section that in most cases, with stringent cuts, the SM background can pretty much be nullified for many cases, and thus these channels can be promising even if the signal cross section is not too high.

While specific models that display the features of charged Higgs couplings displayed in Table I can be interesting in their own right, as mentioned before we postpone such discussions and will present the phenomenology in a completely model-independent way as follows: we will pick the optimal channel for each class of models and do a signal versus background study for an optimal choice of cuts. The signal cross section chosen here is arbitrary, and the only goal here is to finalize a cut flow chart that suppresses the background without substantially affecting the signal cross section. We will then use the number of background events left after imposing the cuts to back calculate the signal cross section necessary for a 5σ discovery. In Sec. IV, we will do a *model-dependent* analysis by translating our results in the parameter space of the type II 2HDM. Specific models with an enlarged scalar sector have many constraints—both theoretical (perturbativity, unitarity) and experimental ($\Delta\rho$, flavor constraints)—that impose various relations between the masses of the new particles and the couplings. While a specific study should certainly cater to these constraints and filter out the parameter space in which to do the phenomenology, our goal here is to provide a sufficiently general analysis that is applicable to wide classes of models, and hence in what follows we will treat the Higgs masses $m_A, m_{H^\pm}$, etc., in a typical multi-Higgs model as essentially independent parameters.

B. Overview of the current experimental limits

The ATLAS and CMS experiments have collected data independently from various phases of the collider run and have looked for a charged Higgs boson, and thus far no conclusive evidence for the same has been found. Below, we collate the results of such findings and briefly discuss each result. One can categorize these search strategies into two cases depending upon the mass of the charged Higgs boson: $m_{H^\pm} < m_t$ and $m_{H^\pm} \geq m_t$. The final state topology, and thus the search strategy, for these two cases is obviously different. Let us begin with the light $H^\pm$ case.

(i) For the $H^\pm \to c\bar{s}$ channel, data have been collected during the different run phases with the integrated luminosity ranging from 4.7 to 19.7 fb^{-1}. From the combined analysis, the mass range 90–160 GeV has been excluded [34,35].

(ii) The CMS Collaboration analyzed the data they collected with $\sqrt{s} = 8$ TeV and the integrated luminosity $\mathcal{L} = 19.7$ fb^{-1} for the decay channel $H^\pm \to c\bar{b}$. No significant excess was found in the mass range 90–150 GeV [36].

(iii) Multiple search analyses have been performed on the $H^\pm \to \tau\nu_\tau$ channel during the different upgrades of the collider. The data which were collected for this study range in integrated luminosity from 2 to 35.9 fb^{-1}. The charged Higgs boson here is produced via top quark decay which in turn is produced in the $t\bar{t}$ production channel. The second top (which did not decay to the $H^\pm$) would further decay to $W^\pm b$ with the $W^\pm$ further decaying to either leptonically or hadronically. The resultant mass exclusion for the case of a light charged Higgs boson from both Collaborations ranges from 80 to 160 GeV [37–39].

For the case of the heavy charged Higgs boson, there are various production channels, i.e., associated production channel $pp \to H^\pm t$, vector boson fusion (VBF) production process and s-channel production, that can each dominate depending on the mass and couplings of the $H^\pm$.

(i) The charged Higgs boson which is produced in the associated production process can further decay leptonically $H^\pm \to \tau^+\nu_\tau$ [40,41] or to top-bottom pair $H^\pm \to tb$ [42]. For the leptonic channel, data have been recorded for the integrated luminosity range 19.5–36.1 fb^{-1}, and masses in the range 180 GeV–3 TeV have been excluded [43]. Further, the hadronically decaying $H^\pm$ has been excluded in the range 200 GeV–2 TeV [44–46].

(ii) The s-channel production process has been analyzed by the ATLAS Collaboration [47] for the integrated luminosity ranging from 20.3 to 36.1 fb^{-1}. In this case, the $H^\pm$ further decays to $W^\pm Z$. The two cases of the electroweak gauge boson decaying semileptonically or fully leptonically have been analyzed, and the charged Higgs mass range 400 GeV–3 TeV has been excluded.

(iii) Vector boson fusion can serve as another significant production channel for the case of heavy charged Higgs. Both ATLAS and CMS Collaborations have collected data for integrated luminosities ranging from 15.2 to 20.3 fb^{-1}. $H^\pm$ produced via the VBF process further decays to a $W^\pm$ and a Z. The CMS Collaboration analyzed events in which both gauge

[2]In this paper, we will only consider single production channels of the charged Higgs. While pair production might be useful in certain models, here we would like to avoid the difficulties involved in reconstruction and the smaller cross sections.

[3]This is, of course, not an absolute necessity, as there is also the possibility that there could be misidentified leptons, etc.

bosons decayed leptonically [48], whereas the ATLAS Collaboration considered that $Z \to \ell^+\ell^-$ and $W^\pm \to qq'$ [49]. The combined mass range which is excluded considering both the analyses ranges from 200 GeV to 2 TeV.

While direct collider limits on the charged Higgs mass seem rather stringent, these limits should be interpreted within the context of *specific* search strategies oftentimes assuming a 100% BR to a desired channel. Thus, for instance, any search involving production or decay processes with a tb would not apply to a chromophobic charged Higgs boson. Thus, in the next sections we will proceed without unduly restraining the charged Higgs mass and analyze the collider phenomenology pertinent to the three broad categories discussed in the previous subsection.

III. COLLIDER PHENOMENOLOGY

In this section we will analyze the $H^\pm$ search prospect for various discovery modes mentioned in Table I at the 14-TeV LHC. As mentioned in the previous section, this analysis will be done without recourse to a particular model in the sense that we will not be using any specific coupling or BR values. However, we will make the following general assumptions about the kinds of models that our analysis applies to:

(i) The scalar spectrum of the model admits, in addition to a charged Higgs, additional neutral scalars (heavier than the SM Higgs). We will generically denote these states by H and A, in keeping with the 2HDM and MSSM notation. In what follows, we will assume that A is lighter than the $H^\pm$ while the H is heavier. We emphasize here that there are no assumptions made about any particular $SU(2)_L \times U(1)_Y$ representation (s) to which these scalars belong.

(ii) We will not employ any specific $\mathcal{CP}$ properties of the H and A; i.e., we will make no assumptions about whether they are scalars or pseudoscalars, as we will not use any angular distribution analyses that will distinguish the two cases.[4]

(iii) For a specific case, say chromophobic, we will assume that all couplings of the $H^\pm$ other than those to colored particles allowed by the SM symmetries are indeed present. This will simplify the analysis as we do not need to make too many model-specific assumptions.

To proceed, we choose three benchmark points $m_{H^\pm} = 300$, 500, and 700 GeV to perform the analysis. The generic production modes of the $H^\pm$ that we will consider are through the decay of the H and the associated production with a top quark. In order to be left with a sufficient number of signal cross sections after the cuts, we have chosen low and moderate values of $m_{H^\pm}$ particularly for the case where it is the decay product of a heavy H. In addition, we fix the masses of the H and A to be 800 and 150 GeV, respectively. We performed the data simulation using the MadGraph5_aMC@NLO [50] event generator. The SM backgrounds which are used for this study are generated via the in-built SM model file in the MadGraph repository. To generate the signal distributions, we built a BSM model file in FeynRules [51,52] with an enlarged scalar sector as detailed in the assumptions above. The parton level simulation from MadGraph were then passed on to the PYTHIA6 [53] program for showering and hadronization. Detector-level simulations of the resulting events were performed with DELPHES3 [54], and the ensuing objects were reconstructed employing the MadAnalysis5 [55,56] framework, which was also used to perform our cut-based analysis that is detailed in the forthcoming sections.

As explained in the preceding sections, we separate the signal into different classes based on the peculiarities of the charged Higgs coupling. While one could fine-tune the phenomenological analysis in each case to cater to its own peculiarities, it is more profitable to exploit the commonalities in the different scenarios so the search strategy is not greatly different. To do so, we first note that the signals presented in Table I can be classified into two classes based upon the exclusive partonic final states available through the decay cascade of the heavier particles produced at LHC: $(2j + 2b + \ell\nu)$ and $(2j + 3b + \ell\nu)$.

In addition to having identical final states, the particles themselves have similar kinematic properties in the two cases because of a common production mode with differences being introduced because of the decay of the $H^\pm$. We see that the leptophobic charged Higgs boson can be looked for in both the channels owing to its unsuppressed tb couplings and gauge interactions. Also, in keeping with Table I, one could also look for pair production of the charged Higgs boson in the chromophobic scenario leading to a different final state from those tabulated above, but we do not pursue it here.

Given the multijet final state, the major experimental search challenges come from dominant SM process like $t\bar{t} + \text{jets}$ and $WZ + \text{jets}$.[5] The presence of $l\nu$ in the signal final state helps in suppressing a large number of pure QCD background events, particularly for signals with appreciable lepton p_T. To begin, we employ the following set of basic identification cuts at the time of simulation to help eliminate any soft jets and leptons:

$$p_T^j > 20 \text{ GeV}, \qquad p_T^\ell > 10 \text{ GeV},$$
$$|\eta^j| \leq 5 \quad \text{and} \quad |\eta^\ell| \leq 2.5. \tag{3.1}$$

[4]However we point out for clarity that we do not include any couplings that is disallowed by $\mathcal{CP}$ symmetry.

[5]Since the signal events have only one source of missing energy, we neglect $ZZ + \text{jets}$ background. However, we have checked that this background gives a negligible contribution once we impose the set of cuts devised.

TABLE II. Classification of signals based on final state topology. The final spectrum has similar kinematic properties in the two cases.

Signal	Chromophobic	Gaugophobic	Leptophobic	Remarks
$2j + 2b + \ell\nu$	✓	✗	✓	Identical production mode. $H^\pm \to W^\pm A$ in chromophobic while $H^\pm \to tb$ in leptophobic.
$2j + 3b + \ell\nu$	✗	✓	✓	Identical production mode. $H^\pm \to W^\pm A$ in leptophobic while $H^\pm \to tb$ in gaugophobic.

TABLE III. Cut flow chart for the $2j + 2b + \ell\nu$ channel with the signal corresponding to a 500 GeV $H^\pm$ in both the chromophobic and leptophobic cases. In the last row, the numbers in brackets correspond to the background when the previous cut on m_{bb} is not applied —this is relevant to the leptophobic case.

	Background		Signal			
Cut	$t\bar{t}$ + jets	WZ + jets	Chromophobic	$\frac{S}{\sqrt{B}}$	Leptophobic	$\frac{S}{\sqrt{B}}$
Initial	2000000	500000	100000	...	100000	...
$N_j \geq 2$	1894836	475313	97053	63.04	97005	65.85
$N_l = 1$	539543	274654	69461	76.97	69590	77.12
$N_b = 2$	163773	11002	24310	58.14	25097	60.03
$H_T \geq 400$ GeV	83444	6124	24038	80.32	24798	82.86
$p_T(j_1) \geq 75$ GeV	70543	5531	22468	81.46	21769	78.92
$p_T(b_1) \geq 75$ GeV	56828	4267	20998	84.95	20740	83.91
120 GeV $\leq m_{bb} \leq$ 180 GeV	11716	477	11716	93.24	...	...
$(m_{H^\pm} - 100)$ GeV $\leq m_{bbjj} \leq (m_{H^\pm} + 100)$ GeV	5893 (20280)	186 (1227)	4333	55.56	6642	45.29

We have chosen a wider window for the pseudorapidity for jets as compared to the leptons to ensure that we do not lose many signal events. Further, we demand that all pairs of particles are optimally separated:

$$\Delta R_{jj} = \Delta R_{bb} = \Delta R_{jl} = \Delta R_{bj} = 0.4. \tag{3.2}$$

With this basic framework now in place, we now turn our attention to optimizing the discovery process of the charged Higgs boson by designing kinematic cuts for the two different final states.

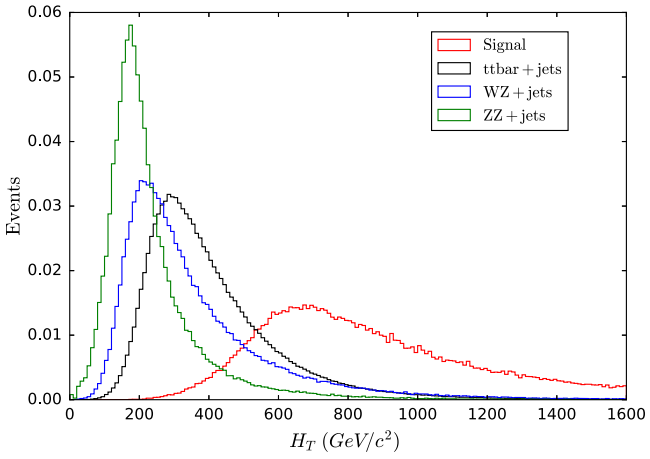

FIG. 1. The $\not{H}_T$ distribution for both signal and background for the chromophobic case for the case of a 500 GeV charged Higgs boson in the $2j + 2b + \ell\nu$ channel. The plot shows that SM background events cluster mostly below 400 GeV in contrast to the signal.

We begin with the $2j + 2b + \ell\nu$ channel—as can be seen in Table II, this applies to both the chromophobic and leptophobic channels. We employ the self-evident set of identification cuts: $N(j) \geq 2$, $N(b) = 2$ and $N(\ell) = 1$. As can be seen from Table III, this will reduce more than 90% of the background, but as collateral damage, we do also lose a large number of signal events. We note at this stage that the signal cross-section numbers given in Table III are fiducial in nature—the purpose of this table is to simply illustrate the efficacy of the cut flow, i.e., systematically eliminate the background without unduly reducing the signal. We reserve all model-specific implications to Sec. IV. The first kinematic quantity which we use to eliminate the background is the total transverse hadronic energy H_T. In the signal all the hadronic particles are produced via the decay of heavily boosted mother particles unlike its SM counterpart. As a result, in Fig. 1, one can notice a wider spread in the signal events (shown for $m_{H^\pm} = 500$ GeV)—this prompts us to choose $H_T \geq 400$ GeV to eliminate the SM background.[6] While the p_T distribution of the leading jets also shows a somewhat similar behavior qualitatively (see Fig. 2)—i.e., the signal has a longer tail while the SM is peaked at lower

[6]Since the distributions are rather similar in both the chromophobic and leptophobic scenarios, we present only the plots for the chromophobic case for illustration purposes.

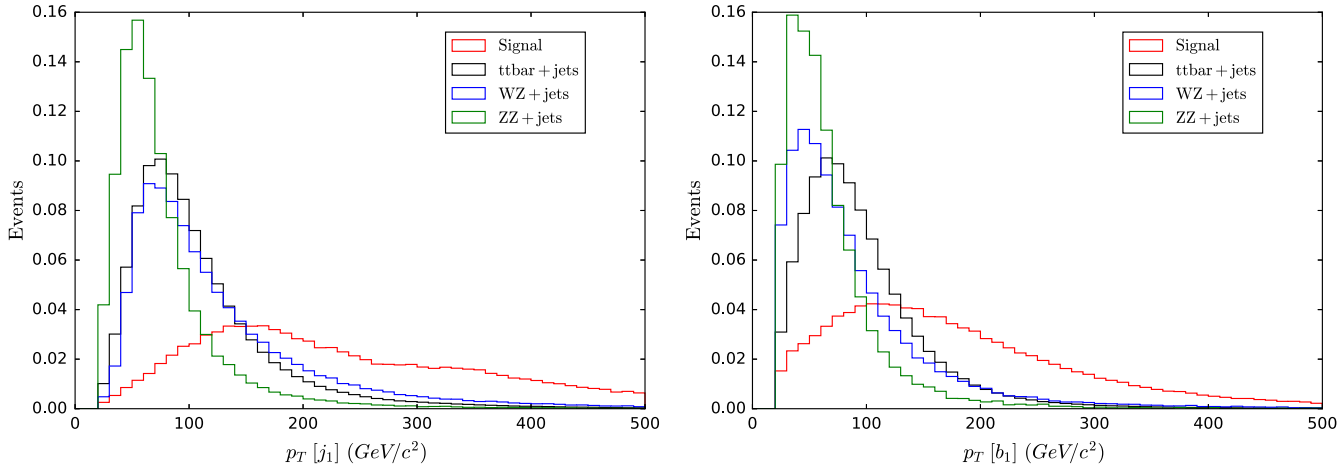

FIG. 2. The p_T distribution for the leading four-flavor jet (left) and the leading b jet (right) in the $2j + 2b + \ell\nu$ channel. The benchmark point of the distribution is $m_{H^\pm} = 500$ GeV.

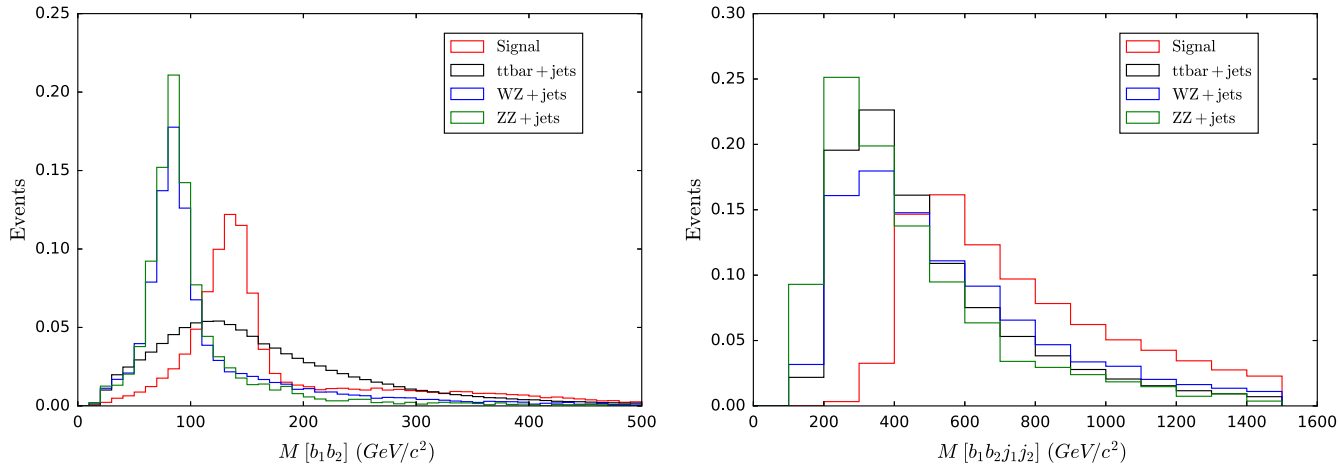

FIG. 3. Invariant mass distributions of m_{bb} (left) and m_{bbjj} (right) for the chromophobic case for a 500 GeV $H^\pm$ in the $2j + 2b + \ell\nu$ channel. It is seen that the m_{bb} distribution for the signal clearly peaks around $m_h = 125$ GeV, while the m_{bbjj} peaks around $m_{H^\pm}$ motivating the cuts given in Table III.

p_T values—imposing hard p_T cuts would run the risk of losing an increased number of signal events in this case. Thus we choose the conservative cuts $p_T(j_1) \geq 75$ GeV and $p_T(b_1) \geq 75$ GeV to achieve an enhanced $\frac{S}{\sqrt{B}}$ ratio, with the p_T's of the subleading jets constrained only by the initial selection cuts.

Finally having thus isolated the signal, we turn to the final step of employing suitable invariant mass cuts. Notice that the chromophobic signal involves a pair of b jets originating from the 150 GeV Higgs boson and the $2b + 2j$ combination that should reconstruct the charged Higgs boson. In the leptophobic case, only the latter condition is true, as the two b jets come from $H^\pm$ and top decay. In Fig. 3, we display both these for the chromophobic signal and background. It is seen that the SM background to $b\bar{b}$ from VV + jets understandably predominantly arises from the decay of the Z, while the $t\bar{t}$ + jets leads to a smoother distribution as the b's in this case result from the hadronic decays of a boosted W. Based on these observations, we choose the cuts 120 GeV $\leq m_{bb} \leq$ 180 GeV and $(m_{H^\pm} - 100)$ GeV $\leq m_{bbjj} \leq (m_{H^\pm} + 100)$ GeV. We note that in the former case we have deliberately chosen a rather asymmetrical cut both to eliminate the background and not lose too much signal in the process based on the distributions in Fig. 3. For the leptophobic case, only the m_{bbjj} cut is applied. This is reflected in Table III as well: in the last column, the numbers in brackets correspond to the background events left after the m_{bbjj} cut when the previous m_{bb} cut is *not* applied.

We present the cut flow chart for the $2j + 2b + \ell\nu$ channel for both the chromophobic and leptophobic scenarios choosing $m_{H^\pm} = 500$ GeV in Table III imposing the cuts discussed in the preceding paragraphs—we see that the progressive kinematic cuts have done a good job in

TABLE IV. Cut flow chart for the $2j + 3b + \ell\nu$ channel with the signal corresponding to a 500 GeV $H^{\pm}$ in both the gaugophobic and leptophobic cases.

	Background		Signal			
Cut	$t\bar{t}$ + jets	WZ + jets	Gaugophobic	$\frac{S}{\sqrt{B}}$	Leptophobic	$\frac{S}{\sqrt{B}}$
Initial	2000000	500000	100000	...	100000	...
$N_j \geq 2$	1894836	475313	97017	63.02	97232	63.15
$N_l = 1$	539543	274654	50763	56.25	51620	57.2
$N_b = 3$	21564	821	13013	86.97	12987	86.8
$H_T \geq 400$ GeV	14800	613	12691	102.22	12702	102.3
$p_T(j_1) \geq 75$ GeV	11204	487	10533	97.41	11634	107.6
$p_T(b_1) \geq 75$ GeV	9723	383	10175	101.21	11153	110.94
$(m_{H^{\pm}} - 100)$ GeV $\leq m_{bbjj} \leq (m_{H^{\pm}} + 100)$ GeV	4734	94	4734	77.29	4458	72.79

TABLE V. The cross sections required for the 5σ and 2σ exclusion of the $m_{H^{\pm}}$ for the different signal scenarios detailed in Tables III and IV for different values of integrated luminosity.

		2σ significance		5σ significance	
Production channel	Benchmark points	$\mathcal{L} = 500$ fb^{-1}	$\mathcal{L} = 1000$ fb^{-1}	$\mathcal{L} = 500$ fb^{-1}	$\mathcal{L} = 1000$ fb^{-1}
Chromophobic	300 GeV	2.997	2.073	7.526	5.31
	500 GeV	2.75	1.939	6.899	4.866
Gaugophobic	300 GeV	2.707	1.912	6.792	4.767
	500 GeV	2.447	1.686	6.151	4.339
Leptophobic $(2j + 3b + \ell\nu)$	300 GeV	2.707	1.912	6.792	4.767
	500 GeV	2.447	1.686	6.151	4.339
Leptophobic $(2j + 2b + \ell\nu)$	300 GeV	5.376	3.8	13.465	9.516
	500 GeV	5.142	3.629	12.995	9.11

systematically suppressing the SM background. In Table IV, we present the corresponding numbers for the $2j + 3b + \ell\nu$ channel for the gaugophobic and leptophobic cases—one can see a similar trend of suppression of the SM in the case as well. In the context of the gaugophobic case, Ref. [42] is particularly relevant—here, the search for a heavy charged Higgs boson is performed in a fashion similar to our discussion of the gaugophobic signal. The dominant background in the experimental study is considered to be $t\bar{t}$ with additional jets along with the subdominant backgrounds diboson $(WW/WZ/ZZ)$ + jets, single top, $Z\gamma$ + jets, $t\bar{t}V$ $(V = W/Z/h)$ and multijet backgrounds. In our study we have restricted ourselves to $t\bar{t}$ + jets and WZ + jets as the dominant background which in some sense agrees with the experimental search strategy, because all the other backgrounds mentioned above have negligible contributions.

Having thus performed a largely model-independent analysis, we now turn to the issue of how large a cross section a particular model should have in order for the charged Higgs boson to be discoverable using the methods outlined above. It is simple enough to take the background events in each case and estimate the actual number of signal events necessary to obtain a 5σ discovery—these numbers are presented for the various scenarios (and for different benchmark points) in Table V. We now turn to the question of realizability of these numbers in the context of a specific model.

IV. MODEL IMPLICATIONS

A. Cross sections and couplings

In the previous sections we have detailed the collider phenomenology of the charged Higgs boson looking at various production and decay channels (see Table I for a quick summary). Combining the various classes of signals based on the final states, we have chosen a set of optimal cuts which help to reduce the corresponding SM background. The number of background events remaining after this set of cuts was then used to back calculate the signal strength necessary for a 5σ discovery—these details are presented in Table V. To truly ascertain the efficacy of the

TABLE VI. The relevant couplings between the charged Higgs boson and the quarks, leptons and bosons in the type II 2HDM.

Vertex	Coupling
$g_{H^\pm W^\mp h}$	$-\frac{ig}{2}\cos(\beta-\alpha)$
$g_{H^\pm W^\mp A}$	$\frac{g}{2}$
$g_{H^\pm qq'}$	$\frac{ig}{2\sqrt{2}m_W}[(m_{q'}\tan\beta+m_q\cot\beta)-(m_{q'}\tan\beta-m_q\cot\beta)\gamma_5]$
$g_{H^\pm\tau\nu}$	$\frac{ig}{2\sqrt{2}m_W}[m_\tau\cot\beta(1-\gamma_5)]$

approach, one needs to analyze the feasibility to realize the signal cross section in a particular model with an enlarged scalar spectrum. While one should, strictly speaking, use models in which the $H^\pm$ is leptophobic, chromophobic, or gaugophobic and compare with the corresponding cross-section numbers, our goal here is not to do an overview of models. Thus, we choose a simpler strategy of choosing a particular model—the type II 2HDM—and turning off the couplings to leptons, colored particles, or gauge bosons to do the comparison in the three cases of interest. The relevant couplings in this model are displayed in Table VI. While we reiterate that the 2HDM does not fall in any of these classes, this analysis should give a sense of the numbers involved and the efficacy of the cuts in each case.

The regions of parameter space that admit a 5σ discovery using the methods outlined in the previous section will obviously depend on the production cross section of the $H^\pm$ and its branching ratios to the relevant final states. While the branching ratios for each case need to be calculated separately, for the purposes of efficient organization of the results, it is useful to note that the charged Higgs boson in both classes of signals is produced either via associated production (gaugophobic and leptophobic cases) or as the decay product of a heavier scalar H (chromophobic and leptophobic cases). We will briefly describe the two channels before moving on to the study of the parameter spaces.

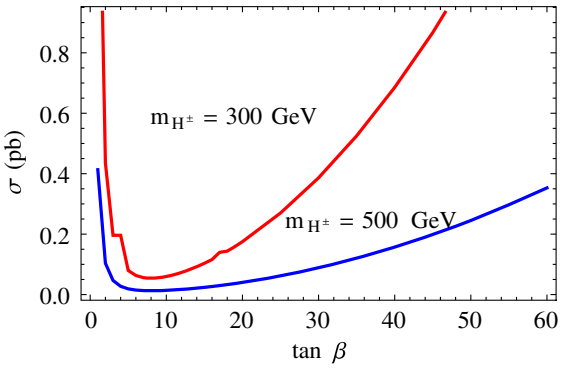

FIG. 4. The plot shows the cross section versus $\tan\beta$ for the case of associated production of charged Higgs $\sigma(gb\to H^\pm t)$ for $m_{H^\pm}=300$ and 500 GeV. The cross section is enhanced for small and large values of $\tan\beta$ and flattens out in the region around $\tan\beta\approx 7$.

Figure 4 shows the cross section as a function of $\tan\beta$ for the associated production process, $\sigma(gb\to H^\pm t)$ at the 14-TeV LHC. The required cross-section values for different charged Higgs mass, $m_{H^\pm}=300$GeV and $m_{H^\pm}=500$ GeV, are collected from the report published by the LHC working group [57]. Referring to Table VI, it is seen that the cross section determined by $g_{H^\pm tb}$ will be enhanced for both small and large values of $\tan\beta$ because of the presence of both $\tan\beta$ and $\cot\beta$ terms—this is borne out by the plot, wherein one can see the enhancement in cross section in the regions $\tan\beta<7$ and $\tan\beta>20$. The region $\tan\beta\approx 7$ affords no such enhancement and is typically the region that is difficult to probe in charged Higgs boson searches in conventional channels. Further, for more massive $H^\pm$, the enhancement in the large $\tan\beta$ region is not as pronounced—thus, in this case, one needs to choose the decay channel of $H^\pm$ pragmatically such that the signal has a high value of $\sigma\times$ BR—we will revisit this issue in the subsequent sections.

The second channel of interest in our study is the production of the $H^\pm$ from the decay of a heavy neutral Higgs H. In order to calculate the cross section $\sigma(gg\to H)$, one can always use the corresponding SM production cross section by a suitably rescaled loop factor [58,59]:

$$\sigma_{\rm 2HDM}(gg\to H)=\frac{\sigma_{\rm SM}\left|\frac{\sin\alpha}{\sin\beta}F^h_{1/2}(\tau_t)+\frac{\cos\alpha}{\cos\beta}F^h_{1/2}(\tau_b)\right|}{|F^h_{1/2}(\tau_t)+F^h_{1/2}(\tau_b)|}, \tag{4.1}$$

where $\tau_f=\frac{4m_f^2}{m_H}$ (with $f=t,\ b$) and the loop factor is $F^h_{1/2}=-2\tau[1+(1-\tau)f(\tau)]$ and

$$f(\tau)=\begin{cases}[\sin^{-1}(1/\sqrt{\tau})]^2 & \tau\geq 1\\ -\frac{1}{4}\left[\ln\frac{1+\sqrt{1-\tau}}{1-\sqrt{1-\tau}}-i\pi\right]^2 & \tau<1.\end{cases} \tag{4.2}$$

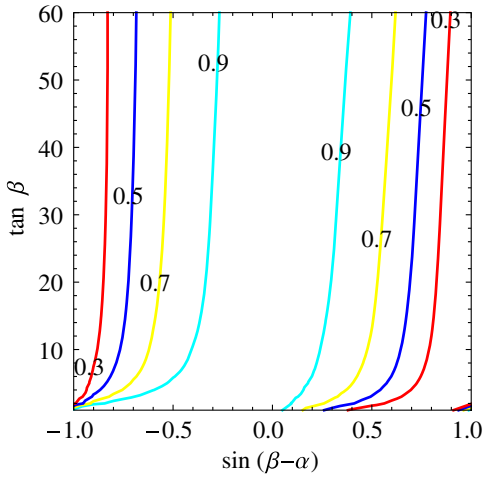

FIG. 5. The plot shows the dependence of production cross section of $\sigma(gg\to H)$ with the free parameter $(\sin(\beta-\alpha),\tan\beta)$. The neutral Higgs boson mass H has been set to $m_H=800$ GeV.

In Fig. 5 we show the dependence of the gluon fusion production cross section with the underline parameter plane $\sin(\beta-\alpha)$ versus $\tan\beta$ fixing $m_H = 800$ GeV. The plot shows the contours of $\sigma_H/\sigma_{\rm SM}$, where $\sigma_{\rm SM}$ is the cross section of the corresponding SM Higgs boson. The cross section is maximal near the $\sin(\beta-\alpha)\approx 0$ regions and does not show appreciable dependence on $\tan\beta$ unlike the associated production channel. The plot is not completely symmetrical about $\sin(\beta-\alpha)=0$—this asymmetry arises due to the complicated loop factors in Eq. (4.1).

B. Discovery and exclusion regions

With the basic structure now in place, we turn to the final question of analyzing the parameter space in the type II 2HDM (with appropriate coupling modifications as discussed earlier) that would permit a 5σ discovery or a 2σ exclusion. We will do this for the three scenarios separately and comment on the results. We point out at the outset that there are many constraints on this model on both the theoretical (vacuum stability, perturbativity, etc.) and experimental (observation of the 125 GeV Higgs, $\Delta\rho$, $b\to s\gamma$, etc.) fronts, and these together constrain the available parameter space of the model. A complete analysis of all such constraints is beyond the scope of this paper (see for example [60]), and thus we present the discovery and exclusion regions on the entire parameter space of type II 2HDM. However, one should note that some of this parameter space might already be ruled out owing to the aforementioned considerations. However, our aim here is to try and understand the maximal available discovery regions for the particular collider analysis detailed in the previous section.

1. Gaugophobic models

Here, the $H^\pm$ is produced via associated production and decays predominantly to $t\bar{b}$—thus, the $g_{H^\pm tb}$ coupling plays a crucial role. In Fig. 6 we show the BR in the tb channel as a function of $\tan\beta$ for two different charged Higgs masses.

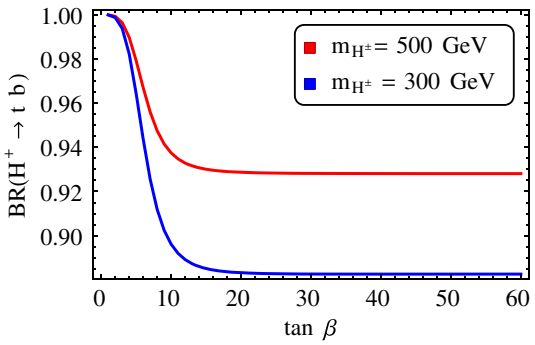

FIG. 6. The plot of the branching ratio of the $H^\pm$ in the $t\bar{b}$ channel for $m_{H^\pm}=500$ GeV (red line) and $m_{H^\pm}=300$ GeV (blue line). The BR is maximal for all values of $\tan\beta$ owing to the absence of the other channels.

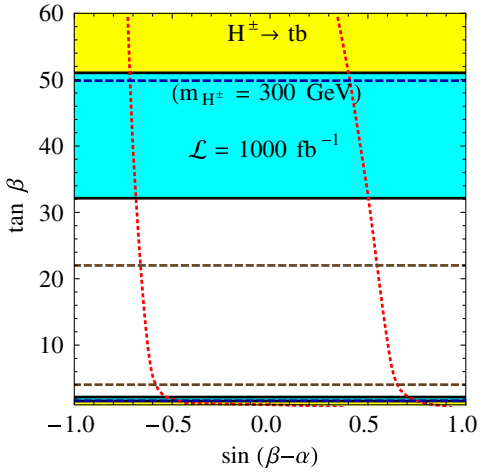

FIG. 7. The 95% exclusion (cyan regions) and the 5σ discovery reach (yellow regions) for the gaugophobic signal for $m_{H^\pm}=300$ GeV. The integrated luminosity is fixed at $\mathcal{L}=1000$ fb^{-1} at the 14-TeV LHC.

It is clear that the absence of the $AW^\pm$ and $hW^\pm$ channels has significantly enhanced this BR, and it is more than ≈90% in the entire parameter space with the only competing channel being $\tau\nu$.

In Fig. 7, we show the contours for discovery and exclusion of a charged Higgs boson in the $\tan\beta-\sin(\beta-\alpha)$ plane for the benchmark value $m_{H^\pm}=300$ GeV and for an integrated luminosity $\mathcal{L}=1000$ fb^{-1}. Bearing out the features of Fig. 4, we see that the discoverable regions are close to $\tan\beta<2$ $\tan\beta>50$. The gaugophobic channel is independent of $\sin(\beta-\alpha)$—we still choose to display the plot so as to be consistent across the different scenarios. From the contour plot, one can see that $4<\tan\beta<35$ is not optimal for charged Higgs boson discovery, as the production cross section is not sufficiently enhanced to overcome the SM background in this region. We find that, consistent with the current experimental results, the channel $gb\to H^\pm t$ is not optimal for charged Higgs boson searches simply because of challenges related to the suppression of the SM background in this case.

While we do not impose all the experimental and theoretical constraints as discussed above, it is instructive to see how the observed rate for $pp\to h\to\gamma\gamma$ constrains the parameter space. This is represented by the dashed red lines—it is seen that only portions of the parameter space close to $\sin(\beta-\alpha)=\pm1$ survive. Specifically, the region between the two dashed red curves is ruled out. This is to be expected, since the h is assumed to be SM-like; its coupling to WW is also close to the SM value which in turn forces $\sin(\beta-\alpha)$ close to ±1.

In addition, in Ref. [42] a lower bound for $\sigma(pp\to H^\pm t)\times{\rm BR}(H^\pm\to t\bar{b})$ of 1.65 pb has been obtained for the case of a 300 GeV charged Higgs boson [considering ${\rm BR}(H^+\to tb)=100\%$]. In a typical 2HDM model, the

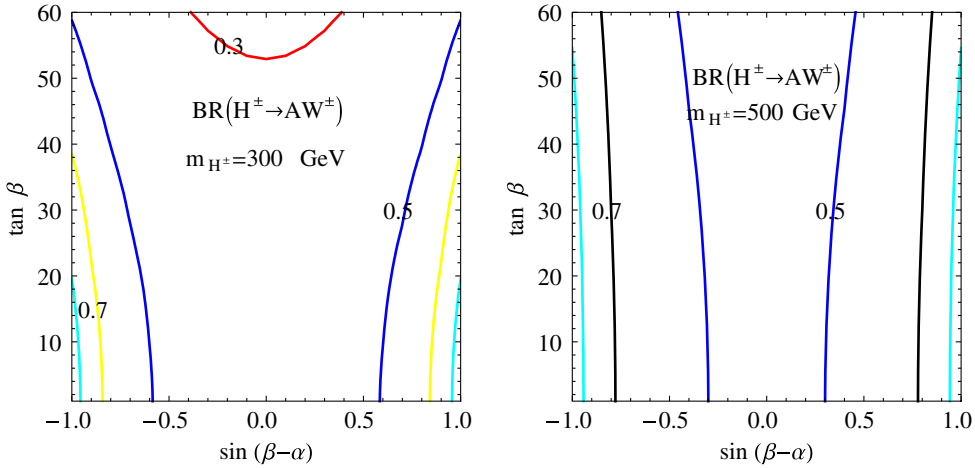

FIG. 8. The contour plot of $H^{\pm} \to W^{\pm}A$ channel for the parameter space $\sin(\beta - \alpha)$ versus $\tan\beta$ for $m_{H^{\pm}} = 300$ GeV (left) and $m_{H^{\pm}} = 500$ GeV (right).

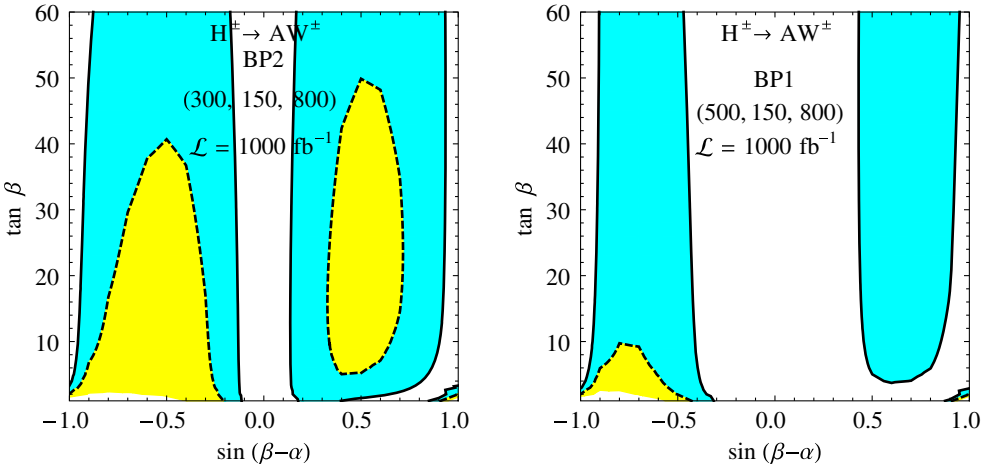

FIG. 9. The 95% exclusion regions (cyan regions) and the 5σ discovery reach (yellow regions) for the chromophobic signal in the $\sin(\beta - \alpha)$ verses $\tan\beta$ plane for the benchmark points 300 (left) and 500 GeV (right).

branching ratio of a charged Higgs boson to tb typically varies from 0.01 to 0.85. The upshot of the conclusions in Ref. [42] as applicable to our case is that regions of parameter space where this branching ratio is more than 10% are excluded. But for a 300 GeV charged Higgs boson, for a large range of $\sin(\beta - \alpha)$ and $\tan\beta$ values, the branching ratio is typically much lower. We have demonstrated this in Fig. 7, wherein we show BR = 1% contours (in dashed brown) and BR = 5% contours (in dashed blue)—it is seen that one can cover a large region of parameter space in the BR < 10% regime.[7]

2. Chromophobic models

In the case of the chromophobic signal, after production via the decay of a heavy scalar, the charged Higgs boson decays to a W boson and a light scalar A. All couplings between $H^{\pm}$ and the colored particle are set to zero in keeping with the chromophobic nature of the charged Higgs boson. In Fig. 8 we present the contour plot of $\mathrm{BR}(H^{\pm} \to W^{\pm}A)$ in the plane $\sin(\beta - \alpha)$ versus $\tan\beta$. From Table I, one can see that the coupling $g_{H^{\pm}W^{\pm}A}$ does not have any dependence on α and β—thus the $\sin(\beta - \alpha)$ and $\tan\beta$ dependence arises due to the total width calculation where one needs to take into account all the available channels for the chromophobic charged Higgs boson.

One can observe from the plot that the BR becomes maximal in the $\sin(\beta - \alpha) \approx \pm 1$ regions. Note that this is in contrast with the cross-section dependence on $\sin(\beta - \alpha)$, which becomes large in the complementary region $\sin(\beta - \alpha) \approx \pm 0$ (Fig. 5). Thus we expect the required $\sigma \times \mathrm{BR}$ for

[7]Note, for example in the two brown contour lines, the regions above the upper contour and the regions below the lower contour are the BR = 1% regions. This is due to the nature of the coupling $g_{H^+tb} = m_t \cot\beta + m_b \tan\beta$.

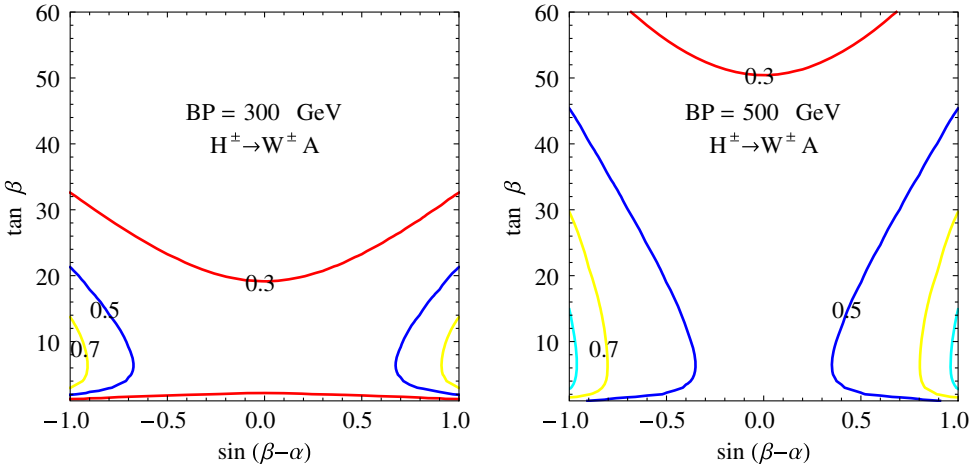

FIG. 10. The contour plot of BR($H^{\pm} \to W^{\pm}A$) in the $\sin(\beta-\alpha)-\tan\beta$ parameter space for $m_{H^{\pm}} = 300$ GeV (left) and $m_{H^{\pm}} = 500$ GeV (right).

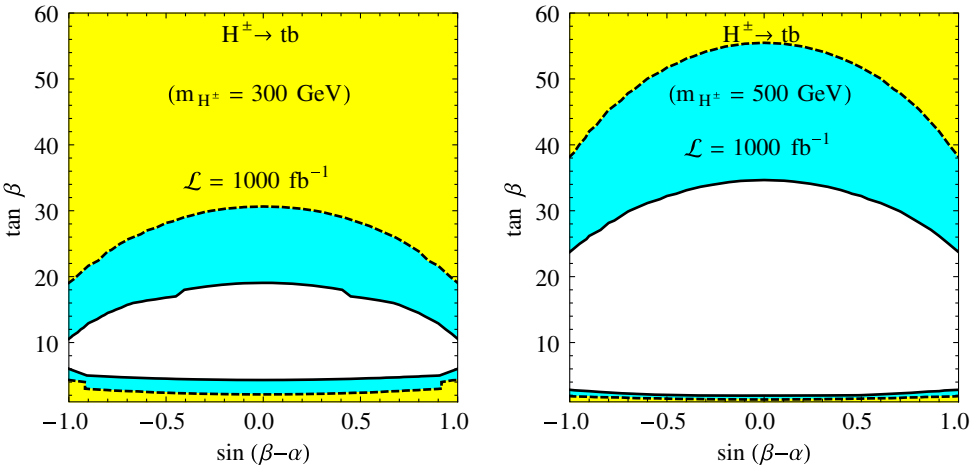

FIG. 11. The 95% exclusion regions (cyan regions) and the 5σ discovery reach (yellow regions) for the leptophobic $3b+2j+\ell\nu$ signal for the benchmark points $m_{H^{\pm}} = 300$ GeV (left) and $m_{H^{\pm}} = 500$ GeV (right). It is seen that the entire range of $\sin(\beta-\alpha)$ for both small and large values of $\tan\beta$ is amenable to discovery.

discovery or exclusion to happen for moderately large values of $\sin(\beta-\alpha)$. In Fig. 9, we present the reach for the chromophobic signal in the $\sin(\beta-\alpha)$ versus $\tan\beta$ plane for the benchmark points 300 and 500 GeV in which this feature is indeed borne out. The 300 GeV case has better reach in the parameter as compared to the 500 GeV due to the higher production cross-section rate. In this case, the $H^{\pm}$ is discoverable in this channel in the regions $-1 < \sin(\beta-\alpha) < -0.2$ and $\tan\beta < 40$ and $0.35 < \sin(\beta-\alpha) < 0.5$ and $6 < \tan\beta < 50$. In the $m_{H^{\pm}} = 500$ GeV case, the discovery region is confined to a small region $-1 < \sin(\beta-\alpha) < -0.4$. Interestingly $\tan\beta = 7$ is a potential discovery region for both benchmark values.[8]

[8]If the charged Higgs is required to decay to a light CP-even Higgs boson, the discovery and exclusion regions are larger than that for the pseudoscalar case discussed here. However, such a light Higgs boson in 2HDM has to be 125 GeV which is not quite the benchmark point we have chosen (150 GeV).

3. Leptophobic models

Leptophobic models can be probed in both the $2b+2j+\ell\nu$ and $3b+2j+\ell\nu$ channels. In the five-jet process, the charged Higgs $H^{\pm}$ decays to a W boson and neutral Higgs A. Hence we need to calculate the branching ratio for $H^{\pm} \to W^{\pm}A$ setting the coupling between $H^{\pm}$ and $\tau\nu$ to zero. In Fig. 10 we present this branching ratio in the parameter plane $\sin(\beta-\alpha)$ versus $\tan\beta$. For the benchmark point $m_{H^{\pm}} = 300$ GeV the branching ratio can be as high as 50% in the region $2 < \tan\beta < 20$ for $\sin(\beta-\alpha) \approx \pm 1$. Further, the BR is at least 30% for the entire range of $\sin(\beta-\alpha)$ for moderately high $\tan\beta$. However, the overall numbers are not as high as in Fig. 8, because the $H^{\pm} \to tb$ (and the decay to other colored particles) takes up a significant amount of the BR. However, it can be seen that, in some regions of parameter space, this can be a viable decay channel to probe. The $m_{H^{\pm}} = 500$ GeV

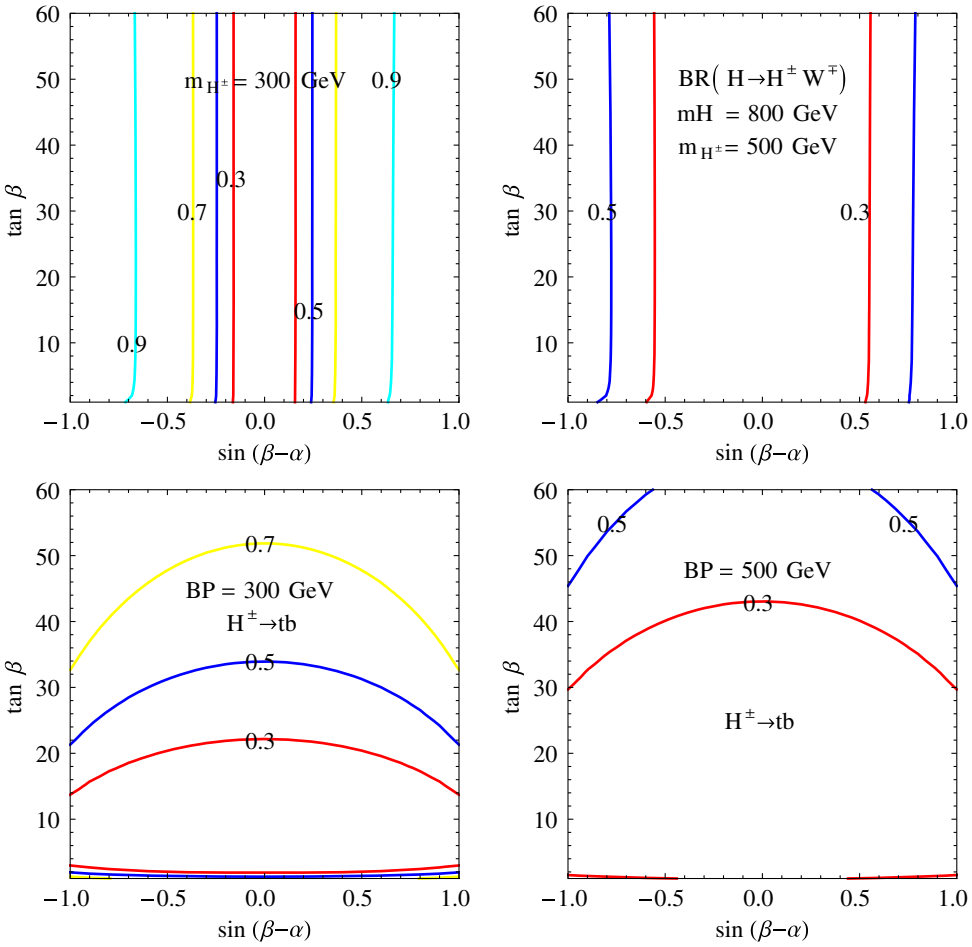

FIG. 12. (Top) Contours of the branching ratio of $H \to H^{\pm}W^{\mp}$ in the $(\sin(\beta-\alpha), \tan\beta)$ plane for $m_H = 800$ GeV and for $m_{H^{\pm}} = 300$ (left) and 500 GeV (right). (Bottom) Contours of the branching ratio of $H^{\pm} \to tb$ for $m_{H^{\pm}} = 300$ (left) and 500 GeV (right).

admits a better branching ratio as compared to the 300 GeV case, as the decay is now more kinematically favored. In Fig. 11, we present the discovery and exclusion reach for this channel for an integrated luminosity of $\mathcal{L} = 1000$ fb^{-1}. Both benchmark points have a potential 5σ discovery reach complementary to the gaugophobic case (which only opened up for very high $\tan\beta$) and the chromophobic case [which did not admit discovery in the region around $\sin(\beta-\alpha) \approx 0$]. While this channel offers the possibility of probing the charged Higgs for a wide range of $\sin(\beta-\alpha)$ values, its reach in terms of $\tan\beta$ is quite limited, again being restricted for small ($\lesssim 4$) or large ($\gtrsim 20$) values. The reach for the $m_{H^{\pm}} = 500$ GeV case is more restricted in spite of the larger branching ratios, because the smaller production cross section for the heavier charged Higgs boson is the decisive factor.

In the leptophobic-four-jets process, the charged Higgs decay is produced via the decay of a heavy scalar H and further decays to tb—thus, in addition to the production cross section of H, the relevant branching ratios for this process are those for $H \to H^{\pm}W^{\mp}$ and $H^{\pm} \to tb$. In Fig. 12, we display contours of these two branching ratios

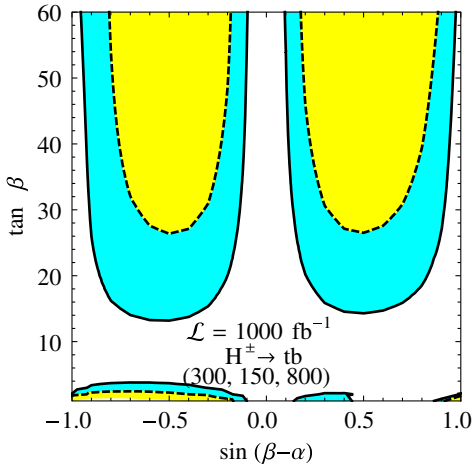

FIG. 13. The 95% exclusion regions (cyan regions) and the 5σ discovery reach (yellow regions) for the leptophobic-four-jets signal in the $\sin(\beta-\alpha) - \tan\beta$ plane for the benchmark point $m_{H^{\pm}} = 300$ GeV and assuming an integrated luminosity $\mathcal{L} = 1000$ fb^{-1} at the 14-TeV LHC. It is observed that the charged Higgs boson is discoverable in this process for $\tan\beta$ values greater than 30.

in the $(\sin(\beta-\alpha), \tan\beta)$ plane for $m_{H^\pm} = 300$ and 500 GeV.

It is seen that while $\mathrm{BR}(H \to H^\pm W^\mp)$ is maximal towards $\sin(\beta-\alpha) = \pm 1$ for all values of $\tan\beta$, the $\mathrm{BR}(H^\pm \to tb)$ is appreciable for large and small values of $\tan\beta$. Remembering that the production cross section of the H (Fig. 5) tends to favor moderately large $\sin(\beta-\alpha)$, we expect the product of these factors to be appreciable over a wide range of $\sin(\beta-\alpha)$ for both large and small values of $\tan\beta$. In Fig. 13, we have presented the discovery and exclusion contours for the charged Higgs boson in this channel for an integrated luminosity of $\mathcal{L} = 1000\ \mathrm{fb}^{-1}$—it is seen that we indeed cover a wide range of parameter space. While the discovery regions for low $\tan\beta$ is rather limited confined to the region $-1 \le \sin(\beta-\alpha) \le -0.2$, those for higher values of $\tan\beta$ are indeed appreciable. As opposed to the chromophobic case, the region $2 < \tan\beta < 10$ is immune to this search owing to the nature of the $g_{H^\pm tb}$ coupling.

V. CONCLUSIONS

Numerous well-motivated extensions of the SM incorporate an enlarged scalar sector with additional neutral and charged Higgs bosons. Now that the SM-like 125 GeV Higgs has been discovered in the ATLAS and CMS experiments, it behooves us to understand the potential of these experiments to unravel signatures of new physics. In this paper, we performed a complete collider analysis to understand the discovery potential of a charged Higgs boson in a model-independent fashion by only assuming certainly general patterns in its coupling to the SM. In this spirit, we classified the charged Higgs boson to be gaugophobic, leptophobic, or chromophobic to understand the discovery reach of the charged Higgs boson in each case. Further, regardless of the pattern of the charged Higgs coupling, we were able to identify and classify the signals broadly in two categories: $2j + 2b + \ell\nu$ and $2j + 3b + \ell\nu$. Accordingly, the model-independent part of the collider analysis dealt with devising effective cuts to suppress the backgrounds for both these processes from all SM sources ($t\bar{t}$ + jets, WZ + jets) to make a 5σ discovery of the $H^\pm$ possible.

Choosing benchmark points of $m_{H^\pm} = 300$ and 500 GeV, we find that the signal cross sections required for the $H^\pm$ discovery ranges between 6 and 13 fb for these different classes of charged Higgs couplings for an integrated luminosity of 500 fb^{-1}, and this range becomes 5–9 fb for $\mathcal{L} = 1000\ \mathrm{fb}^{-1}$. We then proceeded to understand how viable such a scenario is from the point of view of a particular model—which we chose to be the type II 2HDM. We find that in the gaugophobic scenario, where the production and decay of the $H^\pm$ is almost exclusively governed by the $g_{H^\pm tb}$ coupling, one needs very low (≤ 2) or high (≥ 50) $\tan\beta$ for a 5σ discovery of the charged Higgs boson, independent of the value of $\sin(\beta-\alpha)$ for $\mathcal{L} = 1000\ \mathrm{fb}^{-1}$. In the chromophobic case, the efficacy of the analysis depends nontrivially on both $\sin(\beta-\alpha)$ and $\tan\beta$, and the discovery regions cluster around $-1 < \sin(\beta-\alpha) < -0.2$ and $\tan\beta < 40$ and $0.35 < \sin(\beta-\alpha) < 0.5$ and $6 < \tan\beta < 50$. This curious dependence on moderately large $\sin(\beta-\alpha)$ values is because, while the production cross section is enhanced in the small $\sin(\beta-\alpha)$ values, the relevant BR becomes appreciable only for larger values. Most importantly, this scenario admits discovery potential of the $H^\pm$ in the region around $\tan\beta \approx 7$ where traditional searches in the $\tau\nu$ final state typically are difficult. The leptophobic case, while displaying a different qualitative dependence of the discovery region on $\sin(\beta-\alpha)$ and $\tan\beta$ from the gaugophobic case, is similar to it in that one needs very low or very large $\tan\beta$ for discovery. The central point of the analysis is thus rather straightforward: if the charged Higgs boson couples to the colored sector of the SM, the dominant production and decay channels depend strongly on the $g_{H^\pm tb}$ coupling, and hence the features found in the gaugophobic and leptophobic scenarios emerge. If, however, one has an extension of the SM in which the charged Higgs boson does not couple to colored particles (i.e., to tb in particular), one can have markedly different regions of the parameter space that become relevant for collider study.

We conclude this study by pointing out that it is imperative to probe for nonstandard signatures of BSM physics in cases of extended scalar sectors. It is possible that, depending on the nature of the charged Higgs couplings, the discovery of these particles can be effective in channels involving not one, but even two new physics couplings—a case which is usually dismissed as nonviable might indeed turn out to be the dominant discovery mode. In fact, a discovery of the charged Higgs boson in one of these exotic channels might prove to be an efficient way of narrowing down the possibilities of new physics models at the TeV scale.

ACKNOWLEDGMENTS

B. C. acknowledges support from the Department of Science and Technology, India, under Grant No. YSS/2015/001771. The work of S. K. R. is partially supported by funding available from the Department of Atomic Energy, Government of India, for the Regional Centre for Accelerator-based ParticlePhysics (RECAPP), Harish-Chandra Research Institute. S. K. R. would like to thank the Theory Division of CERN while the work was being completed. We thank Satendra Kumar for collaboration during the early stages of this project.

[1] S. Weinberg, Phys. Rev. Lett. **19**, 1264 (1967).
[2] P. W. Higgs, Phys. Rev. Lett. **13**, 508 (1964).
[3] CMS Collaboration, Phys. Lett. B **716**, 30 (2012).
[4] CMS Collaboration, Report No. CMS-PAS-HIG-13-005.
[5] ATLAS Collaboration, Phys. Lett. B **716**, 1 (2012).
[6] ATLAS Collaboration, Phys. Lett. B **726**, 120 (2013).
[7] ATLAS Collaboration, Report No. ATLAS-CONF-2013-034.
[8] B. Heinemann and Y. Nir, Usp. Fiz. Nauk **189**, 985 (2019) [Phys. Usp. **62**, 920 (2019)].
[9] G. C. Branco, P. M. Ferreira, L. Lavoura, M. N. Rebelo, M. Sher, and J. P. Silva, Phys. Rep. **516**, 1 (2012).
[10] C. W. Chiang and K. Yagyu, J. High Energy Phys. 07 (2013) 160.
[11] G. Bhattacharyya and D. Das, Pramana **87**, 40 (2016).
[12] S. De Curtis, S. Moretti, K. Yagyu, and E. Yildirim, Eur. Phys. J. C **77**, 513 (2017).
[13] H. E. Haber, G. L. Kane, and T. Sterling, Nucl. Phys. **B161**, 493 (1979).
[14] M. Aoki, S. Kanemura, K. Tsumura, and K. Yagyu, Phys. Rev. D **80**, 015017 (2009).
[15] H. E. Logan and D. MacLennan, Phys. Rev. D **81**, 075016 (2010).
[16] H. E. Haber and G. L. Kane, Phys. Rep. **117**, 75 (1985).
[17] D. A. Ross and M. J. G. Veltman, Nucl. Phys. **B95**, 135 (1975).
[18] H. Georgi and M. Machacek, Nucl. Phys. **B262**, 463 (1985).
[19] M. S. Chanowitz and M. Golden, Phys. Lett. **165B**, 105 (1985).
[20] C. W. Chiang, arXiv:1504.06424.
[21] H. E. Logan and V. Rentala, Phys. Rev. D **92**, 075011 (2015).
[22] C. Degrande, K. Hartling, H. E. Logan, A. D. Peterson, and M. Zaro, Phys. Rev. D **93**, 035004 (2016).
[23] J. R. Ellis, J. F. Gunion, H. E. Haber, L. Roszkowski, and F. Zwirner, Phys. Rev. D **39**, 844 (1989).
[24] M. Drees, Int. J. Mod. Phys. A **04**, 3635 (1989).
[25] N. D. Christensen, T. Han, Z. Liu, and S. Su, J. High Energy Phys. 08 (2013) 019.
[26] M. Drees, M. Guchait, and D. P. Roy, Phys. Lett. B **471**, 39 (1999).
[27] S. Kanemura, K. Tsumura, K. Yagyu, and H. Yokoya, Phys. Rev. D **90**, 075001 (2014).
[28] C. Englert, E. Re, and M. Spannowsky, Phys. Rev. D **87**, 095014 (2013).
[29] D. Das and A. Santamaria, Phys. Rev. D **94**, 015015 (2016).
[30] A. G. Akeroyd *et al.*, Eur. Phys. J. C **77**, 276 (2017).
[31] A. G. Akeroyd, S. Moretti, K. Yagyu, and E. Yildirim, Int. J. Mod. Phys. A **32**, 1750145 (2017).
[32] U. Maitra, B. Mukhopadhyaya, S. Nandi, S. K. Rai, and A. Shivaji, Phys. Rev. D **89**, 055024 (2014).
[33] R. S. Chivukula, N. D. Christensen, B. Coleppa, and E. H. Simmons, Phys. Rev. D **80**, 035011 (2009).
[34] ATLAS Collaboration, Eur. Phys. J. C **73**, 2465 (2013).
[35] CMS Collaboration, J. High Energy Phys. 12 (2015) 178.
[36] CMS Collaboration, J. High Energy Phys. 11 (2018) 115.
[37] ATLAS Collaboration, J. High Energy Phys. 06 (2012) 039.
[38] ATLAS Collaboration, J. High Energy Phys. 03 (2013) 076.
[39] CMS Collaboration, J. High Energy Phys. 07 (2012) 143.
[40] ATLAS Collaboration, J. High Energy Phys. 03 (2015) 088.
[41] CMS Collaboration, J. High Energy Phys. 11 (2015) 018.
[42] ATLAS Collaboration, J. High Energy Phys. 03 (2016) 127.
[43] CMS Collaboration, Report No. CMS-PAS-HIG-16-031.
[44] ATLAS Collaboration, Phys. Lett. B **759**, 555 (2016).
[45] ATLAS Collaboration, J. High Energy Phys. 09 (2018) 139.
[46] ATLAS Collaboration, J. High Energy Phys. 11 (2018) 085.
[47] ATLAS Collaboration, Phys. Lett. B **787**, 68 (2018).
[48] CMS Collaboration, Phys. Rev. Lett. **119**, 141802 (2017).
[49] ATLAS Collaboration, Phys. Rev. Lett. **114**, 231801 (2015).
[50] J. Alwall, R. Frederix, S. Frixione, V. Hirschi, F. Maltoni, O. Mattelaer, H.-S. Shao, T. Stelzer, P. Torrielli, and M. Zaro, J. High Energy Phys. 07 (2014) 079.
[51] N. D. Christensen, P. de Aquino, C. Degrande, C. Duhr, B. Fuks, M. Herquet, F. Maltoni, and S. Schumann, Eur. Phys. J. C **71**, 1541 (2011).
[52] A. Alloul, N. D. Christensen, C. Degrande, C. Duhr, and B. Fuks, Comput. Phys. Commun. **185**, 2250 (2014).
[53] T. Sjostrand, S. Mrenna, and P. Z. Skands, J. High Energy Phys. 05 (2006) 026.
[54] J. de Favereau, C. Delaere, P. Demin, A. Giammanco, V. Lemaître, A. Mertens, and M. Selvaggi (DELPHES3 Collaboration), J. High Energy Phys. 02 (2014) 057.
[55] E. Conte, B. Fuks, and G. Serret, Comput. Phys. Commun. **184**, 222 (2013).
[56] E. Conte, B. Dumont, B. Fuks, and C. Wymant, Eur. Phys. J. C **74**, 3103 (2014).
[57] S. Dittmaier, M. Kramer, M. Spira, and M. Walser, Phys. Rev. D **83**, 055005 (2011).
[58] A. Djouadi, Phys. Rep. **457**, 1 (2008).
[59] A. Djouadi, Phys. Rep. **459**, 1 (2008).
[60] B. Coleppa, F. Kling, and S. Su, J. High Energy Phys. 01 (2014) 161.